(Table IV and ref 6). Second-shell distances for all other samples are shorter than would be expected for a helical chain of trigonal selenium. This could be due to a change in the pitch of the chain, the presence of six-membered rings, or a chain bending back upon itself. In the case of Se-X-34 and Se-Y-26, the breadth of the second-shell peak in the FT along with the optical and NMR results suggests a mixture of at least two forms of selenium. The helical chains present cannot have a regular Se–Se–Se dihedral angle, or we would expect a sharper distribution of next-nearest-neighbor distances and a higher EXAFS amplitude (Figures 6 and 7). The choice of coordination number becomes somewhat arbitrary when attempting to fit one average interatomic distance to data from several atoms at slightly different distances. In this case the coordination number was fixed at 2. Although this is a good approximation in the case of Se-M-9 and Se-AlPO5-15, where single helical chains occupy the channels, the retained Se–Se next-nearest-neighbor distances for Se-X-26, Se-Y-36, and Se-A-6 represent the weighted-average distance for all allotropes and conformations present in the channels of the molecular sieves.

The loading density of Se in Se-M-9 corresponds to about 3.6 Se atoms per unit cell, which, if it were to adopt the helical-chain allotrope exclusively, would correspond to a chain 6 Å in length per unit cell. When this is compared with the c axial length for hydrated mordenite (7.5 Å), a helical chain would not completely fill the 12-membered-ring channels in mordenite. A similar argument can be extended to Se-AlPO5-15, where 3.5 Se atoms per unit cell corresponds to a chain 5.82 Å in length. Although on the basis of this evidence it is difficult to draw a firm conclusion on the identity of the Se allotrope present, eight-membered rings and bent helical chains must be excluded. The allotrope present is probably a single compressed helical chain in both cases. Interestingly, the 23 wt % loading of Se in mordenite reported elsewhere[11] corresponds to 11.6 Se atoms per unit cell or a chain 19 Å in length or two chains 9.55 Å in length and so on.

Conclusion

The combination of EXAFS and solid-state NMR spectroscopies with optical absorption experiments reveals the effect of spatial confinement of Se in molecular sieves. Encapsulation of Se in various sieves causes the Se–Se bond length to shorten relative to the distance observed in helical chains of trigonal Se. No interchain correlation remains if Se is absorbed in the different sieves, indicating the presence of isolated, single molecular Se_n units. The analysis of the second-nearest-neighbor shell of Se in the one-dimensional (1D) channel systems of mordenite and AlPO5 indicates the highest degree of order of the Se_n units compared to other sieves. Combined with evidence from NMR experiments with AlPO5, loading densities, and optical absorption data, these results are consistent with the presence of a single, highly ordered helical chain allotrope of Se in AlPO5 and mordenite.

The EXAFS data indicate a less restricted next-nearest-neighbor environment in the case of large-pore X and Y, consistent with the presence of a variety of conformations or structures. Optical data support this interpretation, and NMR data suggest that two such structures are present with one probably being helical-chain Se. Optical absorption as well as structural results from EXAFS measurements point to the eight-membered ring allotrope exclusively adsorbed into A zeolite.

Clearly, spatial confinement of semiconducting materials in microporous solids offers much potential for the adjustment of such physical properties as band gaps and optical behavior.

Acknowledgment. We thank Steve Heald, John Tranquada, Jack Scrofani, and Larry Fareria for assistance during data collection. Part of this work was supported by DOE Grant No. DE-AS0580ER10742. C. Yang kindly provided EXAFS data for crystalline Se and As as well as glassy Se.

Registry No. Se, 7782-49-2; AlPO-5, 98499-64-0; mordenite, 12173-98-7.

Contribution from the Laboratoire de Chimie Théorique, Bât. 490, Université de Paris-Sud, 91405 Orsay Cedex, France, and Department of Chemistry, North Carolina State University, Raleigh, North Carolina 27695-8204

Semiconducting Properties of $Li_{0.33}MoO_3$

Enric Canadell*[1a] and Myung-Hwan Whangbo*[1b]

Received August 10, 1987

The bottom d-block band electronic structure of $Li_{0.33}MoO_3$ was derived on the basis of tight-binding band calculations on the Mo_6O_{24} chains that constitute $Li_{0.33}MoO_3$. The distortions of the MoO_6 octahedra in $Li_{0.33}MoO_3$ were analyzed from the viewpoint of the O–Mo···O bond alternation so as to deduce how the t_{2g}-level degeneracy of a regular MoO_6 octahedron is lifted. We found this analysis to be a convenient way of understanding the nature of the bottom d-block bands of $Li_{0.33}MoO_3$. This study suggests that $Li_{0.33}MoO_3$ is a small band gap semiconductor.

Two classes of molybdenum oxide bronzes have been extensively studied because of their low-dimensional structural and electronic properties. The blue bronzes $A_{0.3}MoO_3$ (A = K, Rb, Tl) are two-dimensional (2D) in structure[2] in that they are made up of metal–oxygen layers with composition MoO_3. However, the blue bronzes are quasi-one-dimensional (1D) metals and, as a result, exhibit charge density wave (CDW) phenomena.[3] The purple bronzes $A_{0.9}Mo_6O_{17}$ (A = Na, K) and $TlMo_6O_{17}$ consist of metal–oxygen layers with composition Mo_6O_{17}.[4] Although these purple bronzes are 2D metals, they show CDW phenomena[5] as well. In contrast, the lithium purple bronze $Li_{0.9}Mo_6O_{17}$ differs

(1) (a) Université de Paris Sud. (b) North Carolina State University.
(2) (a) Ghedira, M.; Chenavas, J.; Marezio, M.; Marcus, J. *J. Solid State Chem.* **1985**, *57*, 300. (b) Graham, J.; Wadsley, A. D. *Acta Crystallogr.* **1966**, *20*, 93. (c) Ganne, M.; Boumaza, A.; Dion, M.; Dumas, J. *Mater. Res. Bull.* **1985**, *20*, 1297. (d) Collins, B. T.; Ramanujachary, K. V.; Greenblatt, M.; Waszczak, J. V. *Solid State Commun.* **1985**, *56*, 1023.
(3) (a) Schlenker, C.; Dumas, J. In *Crystal Structures and Properties of Materials with Quasi-One-Dimensional Structures*; Rouxel, J., Ed.; Reidel: Dordrecht, The Netherlands, 1986, p 135. (b) Moret, R.; Pouget, J. P. *Ibid*, p 87. (c) Whangbo, M.-H.; Schneemeyer, L. F. *Inorg. Chem.* **1986**, *25*, 2424. (d) Pouget, J. P.; Noguera, C.; Moudden, A. H.; Moret, R. *J. Phys. (Les Ulis, Fr.)* **1985**, *46*, 1731.
(4) (a) Vincent, H.; Ghedira, M.; Marcus, J.; Mercier, J.; Schlenker, C. *J. Solid State Chem.* **1983**, *47*, 113. (b) Gatehouse, B. M.; Lloyd, D. J.; Miskin, B. K. *NBS Spec. Publ. (U.S.)* **1972**, *No. 364*, 15. (c) Stephenson, N. C. *Acta Crystallogr.* **1966**, *20*, 59. (d) Greenblatt, M.; Ramanujachary, K. V.; McCarroll, W. H.; Neifeld, R.; Waszczak, J. V. *J. Solid State Chem.* **1985**, *59*, 149. (e) Ganne, M.; Dion, M.; Boumaza, A.; Tournoux, M. *Solid State Commun.* **1986**, *59*, 137. (f) Ramanujachary, K. V.; Collins, B. T.; Greenblatt, M. *Solid State Commun.* **1986**, *59*, 647.
(5) (a) Buder, R.; Devenyi, J.; Dumas, J.; Marcus, J.; Mercier, J.; Schlenker, C. *J. Phys. (Les Ulis, Fr.)* **1982**, *43*, L59. (b) Bervas, E.; Cochrane, R. W.; Dumas, J.; Escribe-Filippini, C.; Marcus, J.; Schlenker, C. *Lect. Notes Phys.* **1985**, *217*, 144. (c) Dumas, J.; Bervas, E.; Marcus, J.; Salomon, D.; Schlenker, C. *J. Magn. Magn. Mater.* **1983**, *31–34*, 535. (d) Escribe-Filippini, C.; Konate, K.; Marcus, J.; Schlenker, C.; Almairac, R.; Ayroles, R.; Roucau, C. *Philos. Mag. B* **1984**, *50*, 321. (e) Whangbo, M.-H.; Canadell, E.; Schlenker, C. *J. Am. Chem. Soc.* **1987**, *109*, 6308.

0020-1669/88/1327-0228$01.50/0

from the other purple bronzes both in crystal and in electronic structure.[6] For example, $Li_{0.9}Mo_6O_{17}$ has no separated metal–oxygen layers, but it is a 1D metal[7] despite its three-dimensional (3D) crystal structure.

That a lithium bronze differs in structure from other alkali-metal bronzes with the same composition is also observed in the $A_{0.33}MoO_3$ phase. The red bronzes $A_{0.33}MoO_3$ (A = K, Cs, Rb, Tl)[8] contain metal–oxygen layers with composition MoO_3, different from those layers found in the blue bronzes, and have semiconducting properties that are believed to arise from electron localization.[9] The lithium bronze $Li_{0.33}MoO_3$[10,11] is violet blue and different in crystal structure from the red bronzes. A single-crystal X-ray diffraction study[10a] reveals that $Li_{0.33}MoO_3$ obtained by temperature-gradient techniques[11a,b] is triclinic, quite unique among the known molybdenum bronzes. Nevertheless, triclinic $Li_{0.33}MoO_3$ is found to be a semiconductor.[11a,12] In this work, we analyze how the semiconducting property of $Li_{0.33}MoO_3$ is related to its crystal structure. Thus, we first describe the crystal structure of $Li_{0.33}MoO_3$ and then discuss its electronic structure on the basis of tight-binding band calculations[13] based upon the extended Hückel method.[14] The atomic parameters used in this work are identical with those employed for the band structure calculations on the blue bronze $K_{0.3}MoO_3$[3c] and the purple bronzes $K_{0.9}Mo_6O_{17}$[5e] and $Li_{0.9}Mo_6O_{17}$.[7]

Crystal Structure

Schematically shown in **1** is an Mo_6O_{26} cluster made up of six MoO_6 octahedra sharing their octahedral edges and corners. Such

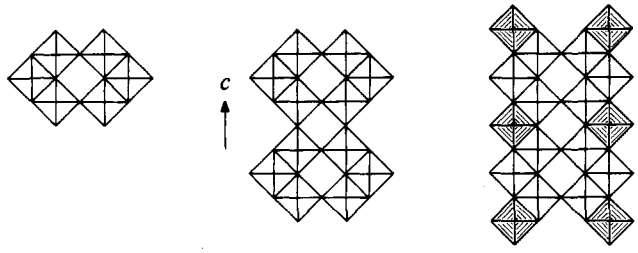

1 **2a** **2b**

Mo_6O_{26} clusters form an Mo_6O_{24} chain **2a** upon sharing their octahedral corners. When LiO_6 octahedra are fused into the Mo_6O_{24} chain between every two adjacent Mo_6O_{26} clusters, one obtains an $Li_2Mo_6O_{30}$ chain **2b**, where LiO_6 octahedra are indicated by shading. Such $Li_2Mo_6O_{30}$ chains share their octahedral corners to form an $Li_2Mo_6O_{28}$ layer **3**. It is these layers that form the 3D crystal structure of $Li_{0.33}MoO_3$ by sharing their octahedral corners and edges. Two $Li_2Mo_6O_{28}$ layers may share their octahedral corners as indicated in **4a** or their octahedral edges as

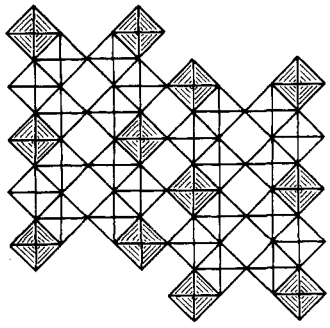

3

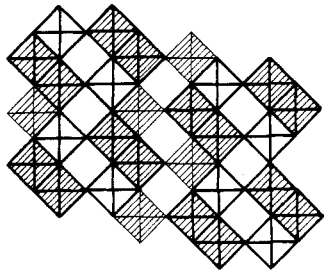

4a

indicated in **4b**, where LiO_6 octahedra of each $Li_2Mo_6O_{28}$ layer

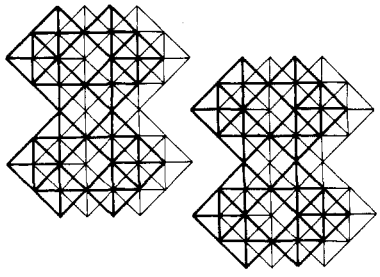

4b

are omitted for clarity. In the layer-stacking **4a**, Mo_6O_{24} chains (**2a**) of one $Li_2Mo_6O_{28}$ layer (**3**) are linked to one another via the Mo_6O_{24} chains of the other $Li_2Mo_6O_{28}$ layer, while this is not the case in the layer-stacking **4b**. In $Li_{0.33}MoO_3$, the types of layer-stacking **4a** and **4b** are both present. As schematically shown in **5**, a unit cell of $Li_{0.33}MoO_3$ contains four shared $Li_2Mo_6O_{28}$

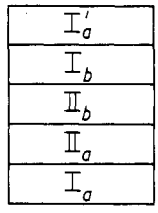

5

layers (I_a, II_a, II_b, and I_b). The layers II_a and II_b share their octahedral edges as in **4b**, while all other adjacent layers share their octahedral corners as in **4a**. Thus, a repeat unit cell of $Li_{0.33}MoO_3$ has the formula unit $(LiMo_3O_9)_8$. Due to the inversion symmetry of the crystal, the layers I_a and II_a are equivalent to I_b and II_b, respectively, so that only two unique $Li_2Mo_6O_{28}$ layers are present in $Li_{0.33}MoO_3$.

Electronic Structure

$Li_{0.33}MoO_3$ has the formula $(LiMo_3O_9)_8$ or four $Li_2Mo_6O_{28}$ layers **3** per unit cell, which is too large for tight-binding band calculations. In discussing the electrical properties of $Li_{0.33}MoO_3$, however, one needs to know only its highest occupied and lowest unoccupied bands. In this section, we derive these bands on the basis of the bottom d-block bands of each $Li_2Mo_6O_{28}$ layer **3** present in $Li_{0.33}MoO_3$.

(6) (a) Onoda, M.; Toriumi, K.; Matsuda, Y.; Sato, M. *J. Solid State Chem.* **1987**, *66*, 163. (b) Schlenker, C.; Schwenk, H.; Escribe-Filippini, C.; Marcus, J. *Physica B+C (Amsterdam)* **1985**, *135B+C*, 511. (c) Greenblatt, M.; McCarroll, W. H.; Neifeld, R.; Croft, M.; Waszczak, J. V. *Solid State Commun.* **1984**, *51*, 671. (d) Ramanujachary, K. V.; Collins, B. T.; Greenblatt, M.; McNally, P.; McCarroll, W. H. *Solid State Ionics* **1986**, *22*, 671. (e) Matsuda, Y.; Onoda, M.; Sato, M. *Physica B+C (Amsterdam)* **1986**, *143B+C*, 243. (f) Sato, M.; Matsuda, Y.; Fukuyama, H., submitted for publication in *J. Phys. C.*
(7) Whangbo, M.-H.; Canadell, E. *J. Am. Chem. Soc.*, in press.
(8) (a) Stephenson, N. C.; Wadsley, A. D. *Acta Crystallogr.* **1965**, *18*, 241. (b) Tsai, P. P.; Potenza, J. A.; Greenblatt, M. *J. Solid State Chem.* **1987**, *69*, 329. (c) Bouchard, G. H.; Perlstein, J. H.; Sienko, M. J. *Inorg. Chem.* **1967**, *6*, 1682. (d) Wold, A.; Kunmann, W.; Arnott, R. J.; Ferretti, A. *Inorg. Chem.* **1964**, *3*, 345.
(9) Travaglini, G.; Wachter, P. *Solid State Commun.* **1983**, *47*, 217.
(10) (a) Tsai, P. P.; Potenza, J.; Greenblatt, M.; Schugar, H. J. *J. Solid State Chem.* **1986**, *64*, 47. (b) McCarroll, W. H.; Greenblatt, M. *J. Solid State Chem.* **1984**, *54*, 282.
(11) (a) Strobel, P.; Greenblatt, M. *J. Solid State Chem.* **1981**, *36*, 331. (b) Nair, K. R.; Wang, E.; Greenblatt, M. *J. Solid State Chem.* **1984**, *55*, 193. (c) Reau, J. M.; Fouassier, C.; Hagenmuller, P. *J. Solid State Chem.* **1970**, *1*, 326.
(12) Greenblatt, M., private communication.
(13) Whangbo, M.-H.; Hoffmann, R. *J. Am. Chem. Soc.* **1978**, *100*, 6093.
(14) Hoffmann, R. *J. Chem. Phys.* **1963**, *39*, 1399. A modified Wolfsberg–Helmholz formula was used to calculate the off-diagonal H_{ij} values: Ammeter, J. H.; Bürgi, H.-B.; Thibeault, J.; Hoffmann, R. *J. Am. Chem. Soc.* **1978**, *100*, 3686.

A. Geometry Distortion and t_{2g}-Level Splitting. The unit cell size $(LiMo_3O_9)_8$ for $Li_{0.33}MoO_3$ suggests that each $Li_2Mo_6O_{28}$ layer **3** has on average only two electrons per unit cell for its d-block bands; i.e., only the lowest lying d-block band is occupied. In identifying the nature of this band and hence constructing the bottom d-block bands of $Li_{0.33}MoO_3$, it is necessary to analyze how the t_{2g}-block levels of a regular MoO_6 octahedron split under the geometrical distortions found in $Li_{0.33}MoO_3$. Shown in **6** are

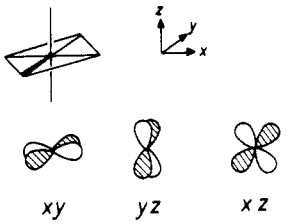

6

the t_{2g}-block levels of a regular MoO_6 octahedron. Though not shown in **6**, the oxygen orbitals of appropriate symmetry combine out of phase with these d orbitals. When the regular octahedron distorts and thus produces a short Mo–O bond, the t_{2g} levels are split in such a way that the levels experiencing more antibonding in the shortened Mo–O bond are raised in energy. Two idealized distortions are shown in **7a** and **7b**, where the Mo atom moves

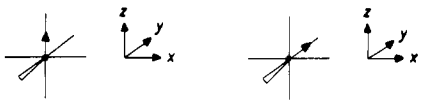

7a **7b**

as indicated by the arrow. The shortening of the "axial" Mo–O bond in **7a** raises the *xz* and *yz* levels, while that of the "equatorial" Mo–O bond in **7b** raises the *xy* and *yz* levels.

In every $Li_2Mo_6O_{28}$ layer of $Li_{0.33}MoO_3$ (e.g., I_a and II_a in **5**), each MoO_6 octahedron has a strong O–Mo···O bond length alternation perpendicular to the layer plane (e.g., ~1.7 vs ~2.4–2.5 Å in Ia and ~1.7 vs ~2.3–2.7 Å in IIa). Thus the *xz* and *yz* orbitals of each MoO_6 octahedron are strongly raised in energy with respect to its *xy* orbital, so that the bottom d-block bands of each $Li_2Mo_6O_{28}$ layer result from the *xy* orbitals of the MoO_6 octahedra. It is important to note that, between adjacent $Li_2Mo_6O_{28}$ layers having the corner stacking shown in **4a**, these *xy* orbitals give rise to δ-type interactions. Since these interactions practically vanish, such $Li_2Mo_6O_{28}$ layers do not interact each other as far as their *xy* orbitals are concerned. As will be discussed in the next section, adjacent $Li_2Mo_6O_{28}$ layers having the edge stacking shown in **4b** (i.e., II_a and II_b in **5**) can also be considered noninteracting as far as their low-lying *xy* bands are concerned. Thus, the bottom d-block bands of $Li_{0.33}MoO_3$ can be approximated by superposing the bottom d-block bands of each $Li_2Mo_6O_{28}$ layer. As discussed already, there are only two unique $Li_2Mo_6O_{28}$ layers (e.g., I_a and II_a in **5**) in $Li_{0.33}MoO_3$. In addition, each layer **3** consists of isolated Mo_6O_{24} chains. Therefore, one needs to calculate only the d-block bands of the Mo_6O_{24} chains present in layers I_a and II_a to be able to derive the bottom d-block bands of $Li_{0.33}MoO_3$.

B. Ideal Mo_4O_8 Chain. In discussing the bottom d-block bands of the Mo_6O_4 chains present in $Li_2Mo_6O_{28}$ layers I_a and II_a, it is convenient to first examine the *xy* bands of the Mo_4O_{18} chain **8**, the noninterrupted portion of the Mo_6O_{24} chain **2a**. Let us

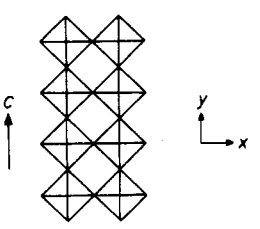

8

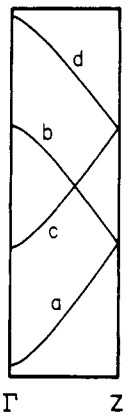

Figure 1. Dispersion relations of the *xy*-block bands for the ideal Mo_4O_{18} chain **8**.

assume that each MoO_6 octahedron of **8** is regular in shape, but we take the four Mo atom cluster Mo_4O_{20} as building blocks of the Mo_4O_{18} chain **8**. Then, the *xy* bands of **8** shown in Figure 1 are constructed from the unit cell orbitals **9a–d**: bands a–d of

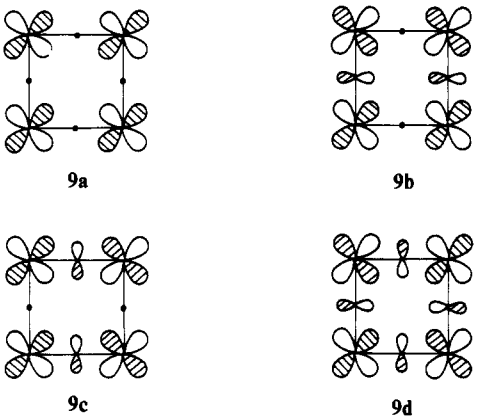

9a **9b** **9c** **9d**

Figure 1 are constructed from the unit cell orbitals **9a–d**, respectively. For example, the orbitals of band a at Γ and *Z* are given by **10** and **11**, respectively, while the orbitals of band b at

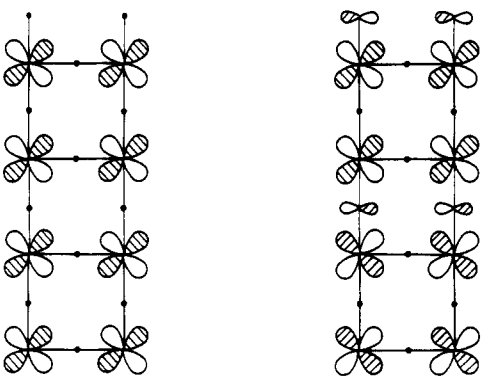

10 **11**

Z and band c at Γ are given by **12** and **13**, respectively.

The d-block band levels of a crystal structure obtained by sharing octahedral corners are raised in energy when the orbitals of the bridging ligand atoms are allowed by symmetry to mix with the metal d orbitals.[5e,7] There are three different types of oxygen bridges in **8**: within a four Mo atom unit cell, two oxygen atom bridges are parallel (∥) to the chain but the other two are perpendicular (⊥) to the chain. Between adjacent unit cells, there are two oxygen bridges parallel to the chain. Summarized in Table I are whether or not the bridging oxygen orbitals mix with the metal d orbitals for the orbitals of the bands a–d at Γ and *Z*. It is clear from **11–13** (and Table I) that band a at *Z*, band b at *Z*, and band c at Γ are all degenerate. Likewise, Table I shows

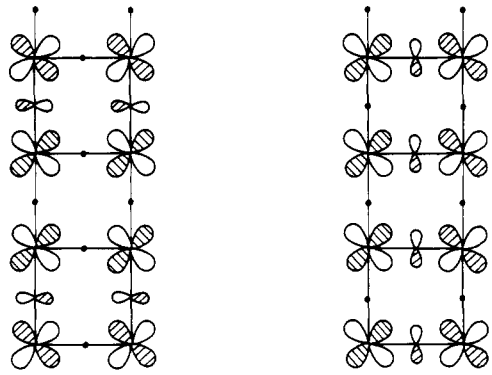

12 13

that band b at Γ, band c at Z, and band *d* at Z are all degenerate. These degeneracies are lifted when the ideal chain **8** is distorted.

C. Real Mo_6O_{24} Chains. Shown in Figure 2 are the bottom portions of the d-block bands calculated for the Mo_6O_{24} chains present in layers I_a and II_a of $Li_{0.33}MoO_3$. These bands are largely derived from the *xy* orbitals of the MoO_6 octahedra and possess dispersion patterns that ressemble those found for the ideal Mo_4O_{18} chain in Figure 1. The band orbital degeneracies of the ideal Mo_4O_{18} chain observed in Figure 1 are all lifted in Figure 2 because of the distortions present in the real Mo_6O_{24}, which will be examined later in this section. The two important features to note from Figure 2 are that the lowest lying band a is separated from other bands lying above either in part a or b of Figure 2 and that the top of band a in Figure 2b lies below the bottom of band c in Figure 2a. With two electrons per unit cell to fill the d-block bands, the band structure of Figure 2a or that of Figure 2b has a band gap, and further, the band structure obtained by superposing parts a and b of Figure 2 also gives a band gap although it is very small.

Let us now discuss how the band dispersion of Figure 2 deviates from that of Figure 1 on the basis of the geometry distortions present in the real Mo_6O_{24} chains. **14a** (**14b**) illustrates how the

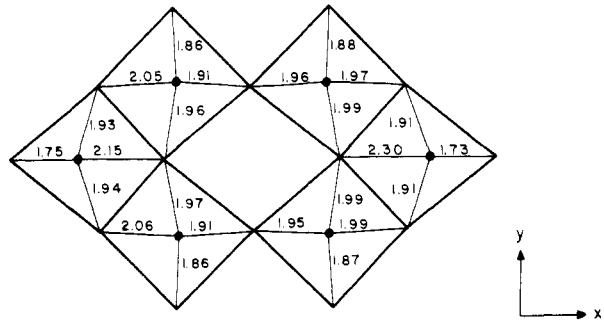

14a

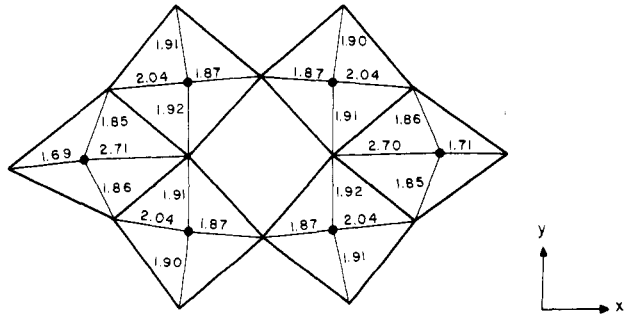

14b

Mo_6O_{26} cluster **1** of the Mo_6O_{24} chain in layer I_a (II_a) of $Li_{0.33}MoO_3$ differs from the corresponding ideal structure constructed from regular MoO_6 octahedra. For simplicity, the Mo–O distances associated with the "axial" oxygen atoms are not shown in **14**. In **14a** and **14b** the "hump" MoO_6 octahedra (i.e., those that are not a part of the Mo_4O_{18} chain **8**) have very short Mo–O distances (~1.7 Å), so that their *xy* orbitals are raised in energy beyond the energy region of Figure 2. Bands b and c in Figure 2 show noncrossing due to the symmetry lowering induced by the distortions. We now comment on why band a at the top of Figure 2b lies slightly lower in energy than band c at the bottom of Figure 2a. The Mo–O bonds in **14a** and **14b** (excluding those of the hump octahedra) approximately "parallel" and "perpendicular" to the Mo_6O_{24} chain may be referred to as the Mo–O (∥) and Mo–O (⊥) bonds, respectively. The average lengths of the Mo–O (⊥) and Mo–O (∥) bonds are respectively 1.92 and 1.97 Å in **14a** and 1.91 and 1.95 Å in **14b**. Since the average Mo–O (⊥) bond length is shorter than the average Mo–O (∥) bond length, the band a top lies below the band c bottom in Figures 2. The average Mo–O (⊥) and Mo–O (∥) bond lengths are both shorter in **14b** than in **14a**, so the band a top and the band c bottom in Figure 2b both lie higher than the corresponding points in Figure 2a. Since the average Mo–O (∥) length in **14b** is longer than the average Mo–O (⊥) length in **14a**, the band a top of Figure 2b lies below the band c bottom of Figure 2a so that band c of Figure 2a does not overlap with band a of Figure 2b.

Finally, we note that band a is essentially obtained from the unit cell orbital **9a**. This orbital has no orbital contribution from the bridging oxygen atoms within a unit cell. In the layer stacking of **4b**, the metal *xy* orbitals of each layer can in principle interact with those of the other layer via the bridging oxygen atoms. However, band a does not have any orbital contribution from the bridging oxygen atoms, so that the character of band a is not expected to change upon the layer stacking of **4b**. Band c is obtained from the unit cell orbital **9c**, which has p-orbital contribution from the O(∥) atoms (i.e., those oxygen atoms on the Mo–O–Mo bridges "parallel" to the Mo_6O_{24} chain) within a unit cell. According to **4b**, these O(∥) atoms of one layer are located on top of the Mo atoms of the other layer so that there exists no overlap between such Mo and O(∥) atoms, Consequently, the

Table I. Antibonding Contributions of the Oxygen p Orbitals of the Mo–O–Mo Bridges in the *xy*-Block Bands of the Mo_4O_{18} Chain[a]

band	unit cell orbital	wave vector point	within a unit cell ∥	within a unit cell ⊥	between unit cells
a	**9a**	Γ	N	N	N
a	**9a**	Z	N	N	Y
b	**9b**	Γ	Y	N	Y
b	**9b**	Z	Y	N	N
c	**9c**	Γ	N	Y	N
c	**9c**	Z	N	Y	Y
d	**9d**	Γ	Y	Y	Y
d	**9d**	Z	Y	Y	N

[a] The presence or absence of the antibonding contribution is indicated by the symbols Y and N, respectively.

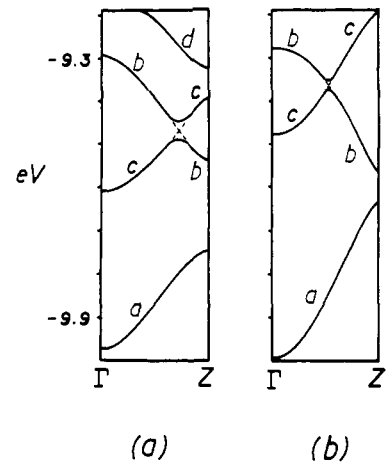

Figure 2. Dispersion relations of the bottom d-block bands calculated for the Mo_6O_{24} chains present in (a) layer I_a and (b) layer II_a.

character of band c is not expected to change upon the layer stacking of **4b**. As a result, the energy gap between band a at Z in Figure 2b and band c at Γ in Figure 2a is expected to remain even if the layer stacking **4b** is taken into consideration. In agreement with this expectation, $Li_{0.33}MoO_3$ is found to be semiconducting in all directions.[12] Since the valence and the conduction bands of Figure 2 are dispersive along $\Gamma \rightarrow Z$, the electrical conductivity of $Li_{0.33}MoO_3$ is expected to be largest along the c direction.

Concluding Remarks

In crystal structure, $Li_{0.33}MoO_3$ differs from other alkali-metal bronzes with the same composition $A_{0.33}MoO_3$ (A = K, Cs, Tl), although it is made up of the same building block, MoO_6 octahedra. By recognizing how the t_{2g}-level degeneracy of a regular MoO_6 octahedron is lifted upon distortion, it is possible to deduce the nature of the bottom d-block bands of $Li_{0.33}MoO_3$, just on the basis of the tight-binding band electronic structures of the Mo_6O_{24} chains that constitute $Li_{0.33}MoO_3$. The present analysis suggests $Li_{0.33}MoO_3$ to be a small band gap semiconductor, which is consistent with the available resistivity data on $Li_{0.33}MoO_3$.

Acknowledgment. This work was supported by NATO, Scientific Affairs Division, and also by DOE, Office of Basic Sciences, Division of Materials Science, under Grant DE-FG05-86-ER45259. M.-H.W. thanks Prof. M. Greenblatt for communication of results prior to publication.

Registry No. $Li_{0.33}MoO_3$, 111556-63-9.

Contribution from the Department of Chemistry, Oregon State University, Corvallis, Oregon 97331, and Isotopes and Nuclear Chemistry Division, Los Alamos National Laboratory, Los Alamos, New Mexico 87545

Dioxygen Difluoride: Electron Diffraction Investigation of the Molecular Structure in the Gas

Lise Hedberg,[†] Kenneth Hedberg,*[†] P. G. Eller,[‡] and R. R. Ryan[‡]

Received July 27, 1987

An electron diffraction study of the structure of dioxygen difluoride (O_2F_2) at −42 °C has confirmed the results of an earlier microwave investigation. The molecule has C_2 symmetry, a short O–O bond, and extraordinarily long O–F bonds: r_g(O–O) = 1.216 (2) Å, r_g(O–F) = 1.586 (2) Å. Other parameter values are $\angle_a$FOO = 109.2 (2)°, $\angle_a$FOOF = 88.1 (4)°, l(O–O) = 0.046 (3) Å, l(O–F) = 0.069 (3) Å, l(O···F) = 0.073 (4) Å, and l(F···F) = 0.113 (10) Å; the l values are rms amplitudes of vibration, and the parameter uncertainties are estimated 2σ. The data are consistent with a high barrier to internal rotation. There is no evidence for the presence of a planar form. Attempts to detect O_2F radical or its dimer were unsuccessful.

Introduction

For some time dioxygen difluoride, hereafter O_2F_2, has been recognized as one of the most potent of all molecular oxidative fluorinating agents.[1] Several years ago it was discovered that O_2F_2 can convert substrates of the actinides U, Np, and Pu to their volatile hexafluorides at effective rates near or below room temperature, i.e. at temperatures 300–400 °C *lower* than those required with any other molecular agents except KrF_2.[2,3] This discovery has important consequences for a number of aspects of nuclear processing and has led to fundamental studies of the properties of O_2F_2.[2,3] The temperature advantage also has significant implications for synthesis of other high-valent, thermally unstable main-group and metallic fluorides.[4]

The structure of O_2F_2 is obviously of considerable interest in connection with its unusual oxidizing properties. A microwave investigation[5] showed the molecule to have a hydrogen peroxide like configuration with a dihedral angle of 87.5°, remarkably long O–F bonds (1.575 Å) compared to those in OF_2 (1.409 Å),[6] and a remarkably short O–O distance—at 1.217 Å only 0.010 Å greater than in dioxygen.[7] The vibrational spectrum of the molecule has been studied many times, and it now appears that uncertainties about some of the assignments[3,8-12] have been removed.[12] Theoretical interest in the molecule has also been stimulated by its unusual structure, but it has been very difficult to predict the observed geometry from quantum-mechanical calculations[13-16] to the accuracy one has come to expect for simple molecules.

Although the geometry of O_2F_2 seemed to have been securely established by the microwave work, the puzzling discrepancy between the microwave results and those from the theoretical calculations merited an additional experimental check by gas-phase electron diffraction. We also wished to investigate the possible presence of an anti form of the molecule and to attempt to obtain diffraction data for the dioxygen fluoride radical O_2F (which results from decomposition of O_2F_2) and for the dimer of the radical, O_4F_2. The O_2F radical is a well-documented species with a long gas-phase lifetime. The dimer has been reported to decompose at low temperature in the condensed phase to give O_2F_2 and O_2.[1]

Experimental Section

Dioxygen difluoride was prepared at Los Alamos[2] and transported to Oregon State in stainless steel cans at liquid-nitrogen temperature for the

[†] Oregon State University.
[‡] Los Alamos National Laboratory.

(1) Streng, A. G. *Chem. Rev.* **1963**, *63*, 607.
(2) Malm, J. G.; Eller, P. G.; Asprey, L. B. *J. Am. Chem. Soc.* **1984**, *106*, 2726. Asprey, L. B.; Eller, P. G.; Kinkead, S. A.; Kissane, R. J.; Foltyn, E. M., submitted for publication in *Inorg. Synth.* Asprey, L. B.; Eller, P. G.; Kinkead, S. A. *Inorg. Chem.* **1986**, *25*, 670. Asprey, L. B.; Kinkead, S. A.; Eller, P. G. *Nucl. Technol.* **1986**, *73*, 69.
(3) Kim, K. C.; Campbell, G. M. *J. Mol. Struct.* **1985**, *129*, 263. Kim, K. C.; Campbell, G. M. *Chem. Phys. Lett.* **1985**, *116*, 236.
(4) Kinkead, S. A.; Asprey, L. B.; Eller, P. G. *J. Fluorine Chem.* **1985**, *29*, 459.
(5) Jackson, R. H. *J. Chem. Soc.* **1962**, 4585.
(6) Morino, Y.; Saito, S. *J. Mol. Spectrosc.* **1966**, *19*, 435.
(7) Huber, K. P.; Herzberg, G. *Molecular Spectra and Molecular Structure*; Van Nostrand: New York, 1979; Vol. IV.
(8) Spratley, R. D.; Turner, J. J.; Pimentel, G. C. *J. Chem. Phys.* **1966**, *44*, 2063.
(9) Loos, K. R.; Goetschel, C. T.; Campanile, V. A. *J. Chem. Phys.* **1970**, *52*, 4418.
(10) Burdett, J. K.; Gardiner, D. J.; Turner, J. J.; Spratley, R. D.; Tchir, P. *J. Chem. Soc., Dalton Trans.* **1973**, 1928.
(11) Jacox, M. E. *J. Mol. Spectrosc.* **1980**, *84*, 74.
(12) Woodruff, W. W.; Larson, E. M.; Swanson, B. I.; Kinkead, S. A.; Jones, L. H.; Eller, P. G.; Kissane, R. J., to be submitted for publication.
(13) Lucchese, R. R.; Schaefer, H. F., III; Rodwell, W. R.; Radom, L. *J. Chem. Phys.* **1978**, *68*, 2507.
(14) Ahlrichs, R.; Taylor, P. R. *Chem. Phys.* **1982**, *72*, 287.
(15) Clabo, D. A., Jr.; Schaefer, H. F., III *Int. J. Quantum Chem.* **1987**, *31*, 429.
(16) Rohlfing, C. M.; Hay, P. J. *J. Chem. Phys.* **1987**, *86*, 4518.

0020-1669/88/1327-0232$01.50/0